HHS Public Access

Author manuscript

Mucosal Immunol. Author manuscript; available in PMC 2019 August 01.

Published in final edited form as:

Mucosal Immunol. 2019 May ; 12(3): 761–771. doi:10.1038/s41385-019-0139-3.

PAD4-dependent NETs generation are indispensable for intestinal clearance of *Citrobacter rodentium*

Piu Saha[1], **Beng San Yeoh**[2], **Xia Xiao**[3], **Rachel M. Golonka**[1], **Vishal Singh**[1], **Yanming Wang**[4], and **Matam Vijay-Kumar**[1,*]

[1]Department of Physiology & Pharmacology, University of Toledo College of Medicine and Life Sciences, Toledo, OH 43614, USA

[2]Graduate Program in Immunology & Infectious Disease, The Pennsylvania State University, University Park, PA 16802, USA

[3]Department of Nutritional Sciences, The Pennsylvania State University, University Park, PA 16802, USA

[4]Center for Eukaryotic Gene Regulation, Department of Biochemistry and Molecular Biology, The Pennsylvania State University, University Park, PA 16802, USA

Abstract

Peptidyl arginine deiminase-4 (PAD4) is indispensable for generation of neutrophil extracellular traps (NETs), which can provide antimicrobial effects during host innate immune response; however, the role of PAD4 against gastrointestinal infection is largely unknown. Herein, we challenged PAD4-deficient (*Pad4*$^{-/-}$) mice and wild-type (WT) littermates with *Citrobacter rodentium* (*CR*), and investigated bacteria clearance and gut pathology. Luminal colonization of *CR* in *Pad4*$^{-/-}$ mice peaked between 11–14 days post-infection, whereas WT mice suppressed the infection by 14 days. We demonstrated that *Pad4*$^{-/-}$ mice were unable to form NETs, whereas WT mice showed increased NETs formation in the colon during infection. *Pad4*$^{-/-}$ mice showed aggravated *CR*-associated inflammation as indicated by elevated systemic and colonic pro-inflammatory markers. Histological analysis revealed that transmissible colonic hyperplasia, goblet cell depletion, and apoptotic cell death were more pronounced in the colon of *CR*-infected *Pad4*$^{-/-}$ mice. Treating WT mice with deoxyribonuclease I, which can disrupt NETs generation, recapitulated the exacerbated *CR* infection and gut pathology associated with the loss of PAD4. Administration of the PAD4 inhibitor, Cl-amidine also aggravated *CR* infection, but to a lesser

*Corresponding Author: Matam Vijay-Kumar (Vijay), PhD, Associate Professor, Department of Physiology & Pharmacology, University of Toledo College of Medicine and Life Sciences, Toledo OH 43614 USA, Off: (419) 383-4130, Fax: (419) 383-2871, MatamVijay.Kumar@Utoledo.edu.

Author contributions:

PS, BSY, and XX performed the experiments and acquired the data; PS, BSY, XX, and RMG conducted the data analyses, results organization, and interpretations; VS performed immunostaining on colonic sections and interpreted the data. PS, MVK designed the research; YW provided the PAD4 deficient mice and participated in the discussion; PS, BSY and MVK wrote the manuscript. MVK guided the entire project.

Disclosures

The authors have no financial conflicts of interest.

extent. Taken together, our findings highlight the importance of PAD4 in the mucosal clearance of *CR* and in resolving gut-associated inflammation.

Keywords

PAD4; Neutrophil extracellular traps; NETs; Deoxyribonuclease I; Infectious colitis

INTRODUCTION

Neutrophil extracellular traps (NETs) are released by neutrophils as a host defense mechanism to trap and eliminate diverse pathogens[1]. The formation of NETs are facilitated by a programmed cell death known as 'NETosis'[2], which is dependent on the reactive oxygen intermediates generated by neutrophil prooxidant enzymes, myeloperoxidase (MPO) and NADPH oxidase (NOX2)[3, 4]. NETosis is initiated by peptidyl arginine deiminase-4 (PAD4, aka *Padi4*), an enzyme that catalyzes the removal of the positively-charged -NH_2 group on arginine residues of histone 3 (H3), thus forming citrullinated H3 (H3Cit). This allows chromatin to decondense and thus released as web-like structures decorated by an array of antimicrobial proteins[5]; however, genetic loss of PAD4 abrogates the formation of these NETs[6]. Accordingly, PAD4-deficient (*Pad4*$^{-/-}$) mice have been employed as the *in vivo* model to demonstrate the role of NETs in various pathological conditions such as wound healing[7], deep vein thrombosis[8], bacterial infection and sepsis[6, 9], and myocardial[10] and liver injury[11]. Despite the increasing scientific endeavors to target PAD4 in treating various diseases, the role of PAD4 in gastrointestinal (GI) infections is severely under-explored.

Citrobacter rodentium (*CR*) is a Gram-negative murine enteropathogen, which causes attaching and effacing (A/E) lesions in the distal part of the gut[12]. *CR* primarily colonize the cecal and colonic epithelia, resulting in diarrhea, goblet cell loss and immune cell infiltration such as macrophages and neutrophils, which promote intestinal inflammation[12]. Although *CR* causes high mortality in sucklings, the course of infection is self-limiting[13] and precipitates transmissible colonic hyperplasia in adult mice[14, 15]. Accordingly, this infection model has been widely used to study the pathogenesis of two clinically important human GI pathogens, i.e. enteropathogenic *E. coli* (EPEC) and enterohaemorrhagic *E. coli* (EHEC)[13]. Moreover, this model has been utilized to better understand the pathogenesis of various intestinal disorders, i.e. infectious colitis, inflammatory bowel diseases and tumorigenesis[16].

Several studies demonstrate that neutrophils are essential for protection against *CR* infection[17, 18], where depletion of neutrophils increased dissemination of bacteria and mortality in mice[17]. However, the role of the neutrophilic enzyme, PAD4 against *CR* infection remains to be investigated. Herein, we studied the significance of PAD4 in limiting *CR* infection by employing *Pad4*$^{-/-}$ mice. Our results demonstrated that mice lacking PAD4 are unable to form NETs whereas WT mice displayed increased NETs formation in the colon in response to *CR* infection. Such impairment in *Pad4*$^{-/-}$ mice was associated with a delayed clearance of *CR* even after 28 days post-infection (p.i), whereas WT mice managed to clear the infection. In addition, *Pad4*$^{-/-}$ mice also developed a severe intestinal pathology

evidenced by increases in colonic hyperplasia and apoptotic cell death that could be due, in part, to their prolonged infection when compared with WT mice. Pharmacological interventions, via administration of deoxyribonuclease I (DNase I) to degrade NETs or Cl-amidine to inhibit PAD4 activity, aggravated *CR* infection in WT mice and recapitulated the intestinal pathology associated with the loss of PAD4. Taken together, our findings underscore the critical role of PAD4 and NETs in ensuring timely clearance of *CR* and conferring protection from the GI pathology associated with the infection.

RESULTS

PAD4 deficiency impaired NETs formation and clearance of *C. rodentium* infection

To examine the role of PAD4 against gastrointestinal infection, *Pad4*$^{-/-}$ mice and their WT littermates were challenged with *CR* (1×10^9 CFU) intragastrically and monitored for 28 days. Both groups developed loose stools that were indicative of diarrhea (data not shown), but no apparent loss in body weight was observed (Fig. 1A). Nonetheless, *Pad4*$^{-/-}$ mice displayed more fecal shedding of *CR* after day 4 onward up to day 16 p.i. and gradually resolved from day 20–28 p.i. (Fig. 1B). To address whether the increased fecal shedding of *CR* was due to their greater capacity to colonize the GI tract, we euthanized the mice and measured *CR* burden in the gut and other organs. Indeed, *CR* burden was substantially higher in the cecal content, spleen and mesenteric lymph nodes (MLNs) of *Pad4*$^{-/-}$ mice than WT mice at day 10 p.i. (Supplemental Fig. 1A–C). When compared to WT, *Pad4*$^{-/-}$ mice displayed a pronounced splenomegaly, loss of cecum weight and colomegaly at day 10 p.i. (Supplemental Fig. 1D–F) and day 28 p.i. (Fig. 1C, D). Such outcomes indicate that the loss of PAD4 not only worsened *CR* infection in the gut, but also increased their dissemination to extra-intestinal organs.

PAD4 deficiency also impeded proper clearance of *CR* and allowed the pathogen to persist in the gut, spleen and MLNs of *Pad4*$^{-/-}$ mice through day 28 p.i.. At this time, WT mice had substantially recovered from the infection with minimal to no detectable levels of *CR* in fecal shedding and any of the tissues analyzed (Fig. 1E–H). Taken together, these results highlight the mucoprotective role of PAD4, which is necessary for restricting *CR* colonization in the GI tract and facilitating its clearance during the course of infection.

To visualize colonic NETs formed during *CR* infection, we immunostained colon sections from control and *CR*-infected mice for H3Cit (a defining marker for NETs), Ly6G (neutrophil marker) and DNA (DAPI, a nucleus binding dye). Our results showed that WT mice displayed minimal H3Cit positivity at baseline (Fig. 1I), but were capable of upregulating colonic H3Cit following *CR* infection (Fig. 1J). The pattern of H3Cit staining in *CR*-infected WT mice resembled web-like structures and was co-localized with Ly6G staining, thus suggesting that they are likely to be a part of NETs. However, such structures were absent in both uninfected and *CR*-infected *Pad4*$^{-/-}$ mice (Fig. 1K–M). Interestingly, we observed few instances of H3Cit positivity in *Pad4*$^{-/-}$ mice; however, their lack of strand-like features indicate that they were unlikely to be NETs. Rather, we postulate these staining could be an artifact or a result of H3 citrullinated by other PAD isoforms that are not involved in NETs formation.

Pad4$^{-/-}$ mice exhibited persistent exacerbated inflammation during *C. rodentium* infection

Considering that gut inflammation is a typical sequela of *CR* infection, we next asked whether such inflammation could be exacerbated in *Pad4*$^{-/-}$ mice that failed to clear *CR* in a timely manner. To address this possibility, we first measured the levels of fecal Lcn2, a sensitive biomarker for gut inflammation[19], at different time points of p.i.. As anticipated, fecal Lipocalin 2 (Lcn2) was significantly elevated in *Pad4*$^{-/-}$ mice in a trend similar to the levels of *CR* fecal shedding, which peaks at 10 days p.i. (Fig. 2A). Likewise, systemic markers of inflammation [serum Lcn2, serum amyloid A (SAA)] and neutrophil signature markers [neutrophil elastase (NE), myeloperoxidase (MPO)] were more elevated in *CR*-infected *Pad4*$^{-/-}$ mice than WT mice (Fig. 2B–E). The expression of colonic inflammatory markers, i.e. tumor necrosis factor (*TNF-α*), keratinocyte-derived chemokine (*KC*), interleukin (*IL*)-*17, IL-1β*, *IL-6*, interferon-*γ* (*IFN-γ*) and inducible nitric oxide synthase (*iNOS*), were similarly upregulated in *Pad4*$^{-/-}$ mice at day 10 p.i. (Supplemental Fig. 2A–G).

The cytokines, IL-22 and IL-17A, are produced by T cells that have been shown to mediate early mucosal host defense against bacterial infection[20, 21]. Although the colonic levels of these cytokines were elevated in both *CR*-infected WT and *Pad4*$^{-/-}$ mice at day 10 p.i., their upregulation was more pronounced in the latter (Fig 2F, G). Analysis on colonic lamina propria immune cells showed that CR infection significantly increased Th17 (CD3+CD4+RORγt+) cells in WT and Pad4−/− mice (Fig. 2H), albeit less Th17 cells were observed in Pad4−/− mice when compared to WT mice; however, we did not observe any significant difference in Treg cells ($CD4^+CD25^+FoxP3^+$) in both groups (Fig. 2I). Interestingly, colonic IL-22 and IL-17A levels were subsequently dampened in both *CR*-infected WT and *Pad4*$^{-/-}$ mice at day 28 p.i (Fig. 2J, K). Considering that mucosal IgA is also a key factor in facilitating *CR* clearance[22, 23], we next asked whether *Pad4*$^{-/-}$ mice display any impediment in their IgA response. In contrast, fecal IgA was substantially elevated in *Pad4*$^{-/-}$ mice after day 16 p.i. and persisted to day 28 p.i., when compared to the mildly elevated fecal IgA levels in WT mice (Fig. 2L). Such heightened immune responses in *CR*-infected *Pad4*$^{-/-}$ mice may be regarded as part of a compensatory mechanism, *albeit* inadequate to offset the loss of antimicrobial immunity due to PAD4 deficiency.

C. rodentium infection led to significant colonic hyperplasia in *Pad4*$^{-/-}$ mice

Histological analysis further revealed that, compared to WT mice, the colons of infected *Pad4*$^{-/-}$ mice had substantially increased epithelial ulceration, crypt elongation and hyperplasia, thickening of the mucosa, and depletion of goblet cells at day 28 p.i. (Fig. 3A–D). These features are typical hallmarks of *CR*-induced goblet cell loss[25] and transmissible colonic hyperplasia due to rapid epithelial proliferation, regeneration and repair mechanisms[13]. A similar trend in the above histological parameters were also observed in the colon of *CR*-infected *Pad4*$^{-/-}$ mice analyzed at day 10 p.i (Supplemental Fig. 3A–C). In addition, we observed a significant increase in apoptotic cell death, visualized via TUNEL (terminal deoxynucleotidyl transferase dUTP nick end labeling) staining, in the colonic crypts of *Pad4*$^{-/-}$ mice compared with WT mice at day 28 p.i.. Intriguingly, *Pad4*$^{-/-}$ mice also displayed a higher basal level of apoptosis in colonic crypts, whereas very few apoptotic cells were observed in the crypts of WT mice (Fig 3E–G). Collectively, these outcomes

suggest that PAD4 deficiency may also impact cell survival in the colon, though further studies are needed to confirm which cell-types were affected.

The colonic pathology induced by *CR* infection is often associated with the loss of epithelial barrier integrity, thus increasing systemic dissemination of other gut bacteria[24]. To confirm this possibility, we determined the serum immunoreactivity to microbial products in *CR*-infected mice as a surrogate measure of bacterial translocation. As anticipated, we observed increased levels of IgG generated against *E. coli* proteins (Fig. 3H), in addition to bacterial LPS and flagellin (Supplemental Fig. 3D, E). Such increased permeability to bacteria and their products, in part, substantiate the susceptibility of *Pad4*$^{-/-}$ mice to increased *CR* dissemination during infection.

C. rodentium colonized the gastrointestinal tract more rapidly in *Pad4*$^{-/-}$ mice

To visualize the kinetics of *CR* colonization over the course of infection, we challenged WT and *Pad4*$^{-/-}$ mice with a bioluminescent strain of *CR* (ICC180). Mice were fed with alfalfa-free, compositionally-defined purified diet for the duration of this study to minimize the background florescence from the chlorophyll and other pigments present in grain-based chow. The low levels of *CR* bioluminescence in WT mice was observed to expand from day 1 to 7 p.i. and subsequently receded from day 9 to 14 p.i.. In comparison, *Pad4*$^{-/-}$ mice displayed a notably more diffuse pattern of *CR* bioluminescence that intensified from day 3 p.i. onward and persisted to day 14 p.i (Fig. 4A, B). In line with our earlier observations, the inflammation was more severe in *Pad4*$^{-/-}$ than WT mice as evident by the gross colon, splenomegaly, colomegaly and enlarged MLNs (Supplemental Fig. 4A–E). However, there was no loss in body weight between the groups (data not shown). Analysis of *CR* burden in the spleen, MLNs, cecal content and fecal shedding were consistent with our overall observation that loss of PAD4 increased the susceptibility to *CR* colonization and dissemination (Supplemental Fig. 4F–I). Histological analysis showed the aggravated colonic histopathology, goblet cell depletion and submucosal edema in *CR*-infected *Pad4*$^{-/-}$ mice (Supplemental Fig. 4J).

Disruption of NETs aggravated the susceptibility to *C. rodentium* infection

One of the well-characterized role of PAD4 is to initiate the formation of NETs, a web-like structure comprised of neutrophil DNA[6, 26]. Accordingly, the susceptibility of *Pad4*$^{-/-}$ mice to *CR* infection could be potentially due to their inability to generate NETs for trapping, killing and preventing the dissemination of this pathogen. If that is the case, we envisioned that administration of exogenous DNase I to degrade NETs in *CR*-infected WT mice could recapitulate the aggravated infection and inflammation seen in *Pad4*$^{-/-}$ mice. We did not observe any body weight difference between *CR*-infected WT mice with and without DNase I treatment (Fig. 5A). Yet, DNase I-treated mice displayed progressively increasing *CR* burden in fecal shedding from day 4 p.i. onwards (Fig. 5B, C). DNase I treatment also increased CR burden in the ceca by day 11 p.i. (Fig. 5D). There is an increasing trend in CR dissemination to the spleen, albeit not reaching significance (Fig. 5E). In line with the exacerbated infection, DNase I-treated mice also developed more severe inflammation as evident by their significantly elevated fecal Lcn2, serum Lcn2 and SAA (Fig. 5F–H).

Histological analysis affirmed the worsened colonic histopathology, marked by goblet cell depletion and submucosal edema in the DNase I-treated mice (Fig. 5I, J).

Next, we asked whether pharmacological inhibition of PAD4 in mice could also increase their susceptibility to *CR* infection. Cl-amidine is a water-soluble, cell-permeable pan-PAD inhibitor that inactivates the enzymatic activity of PAD4 by irreversibly modifying its active site cysteine residue[27]. Treating *CR*-infected WT mice with Cl-amidine did not result in body weight loss, but elevated *CR* burden in the fecal shedding and fecal Lcn2 levels with an increasing trend in serum Lcn2 (Fig. 6A–D). However, *CR* burden in the spleen and MLNs was comparable between vehicle and Cl-amidine treated mice (data not shown). Mice given Cl-amidine nonetheless partially recapitulated the colon histopathology seen in *Pad4*$^{-/-}$ mice (Fig. 6E, F), albeit to a lesser extent in severity. Collectively, the findings of this study implicates the importance of PAD4 and NETs formation against *CR* infection, whereas their loss of function either via genetic deficiency or pharmacologic intervention could worsen the disease.

DISCUSSION

C. rodentium (*CR*) is one attaching-effacing enteropathogen that transiently infects the murine gut and elicits colonic hyperplasia that are reminiscent of EPEC and EHEC infections in humans. Accordingly, *CR* has been widely-employed as a model of gut mucosal infection to elucidate the various host-pathogen crosstalk[28] that could be targeted to promote recovery following infection. Among the innate immune cells, neutrophils are the first responder cell-type that institute a first-line of defense against diverse pathogens[29]. Several lines of evidence suggest that neutrophils are indispensable during *CR* infection[17, 30] whereby their depletion increases systemic dissemination of *CR* and mortality[17]. Timely recruitment of neutrophils to the site of *CR* infection has been shown to be dependent on the chemokines released following the activation of pathogen recognition receptors[31, 32] and MyD88 signaling[17, 33]. Incidentally, the loss of chemokine receptor, CXCR2, has been shown to disrupt mucosal influx of neutrophils, which in turn aggravated the colitis-associated diarrhea caused by *CR*[34]. Notwithstanding the well-appreciated role of neutrophils against *CR*, it is still unclear whether PAD4 and/or NETs are indispensable for facilitating *CR* clearance and mucosal restitution.

A prevailing paradigm proposes that the formation of NETs requires the activity of PAD4, which removes the positively-charged -NH_2 group on the arginine residues of histone 3 (H3) to allow the chromatin to unwind and be released as NETs[26]. Although the DNA itself has antimicrobial properties[35], its primary role in NETs is to entrap the encroaching bacteria while leaving them vulnerable to the bactericidal activity of various neutrophil proteins decorating the NETs[36, 37]. Mice deficient in PAD4, however, have been shown to be incapable of forming NETs and thus are more susceptible to bacterial infection[6]. However, the endeavor to visualize NETs in inflamed tissues remains challenging as the contemporary methodologies used to assess NETs *in vitro* are not feasible for *in vivo* study. To address this limitation, we probed for H3Cit as a surrogate, if not a definitive marker, for NETs released in the intestine. Our results illustrated the presence of colonic H3Cit decorating the mesh-like structures, which we presumed to be NETs following *CR* infection. Such contention is

supported by our observation that (i) H3Cit co-localized with $Ly6G^+$ neutrophils and that (ii) such features were absent in *Pad4*$^{-/-}$ mice.

In this study, we found evidence that *Pad4*$^{-/-}$ mice were not able to subdue *CR* infection in the gut, resulting in increased pathogen burden and dissemination. This notion was substantiated via IVIS imaging of the bioluminescent *CR*, which exhibited a diffuse pattern that expanded more rapidly in *Pad4*$^{-/-}$ mice when compared to WT mice. *Pad4*$^{-/-}$ mice also displayed a more severe colonic hyperplasia and apoptosis that were likely due, in part, to their prolonged infection and the inability to adequately clear the pathogen. Intriguingly, the fecal shedding of *CR* in *Pad4*$^{-/-}$ mice gradually decreased after the peak of infection around day 12–16 p.i. This decline in *CR* burden at the later time points could be potentially due to the participation of other immune responses, such as upregulation of colonic IL-22 and IL-17A observed at day 10 p.i. and the elevation of fecal IgA levels that occured after 16 day p.i. Such notion is in line with previous reports demonstrating the importance of IL-22 and IL-17A as antimicrobial cytokines, which confer protection against *CR* infection[20, 21, 38]. Moreover, the adaptive immune response (T and B cells) also participates in clearing *CR* infection[23, 39], *albeit* delayed. Such responses, though beneficial to promote *CR* clearance at later time points, were insufficient to compensate for the loss of PAD4 and/or NETs, especially in regards to alleviating the extent of colonic injury and inflammation incurred by *CR* infection.

Though the pathology observed in *Pad4*$^{-/-}$ mice can be largely attributed to NETs deficiency, such a presumption needs to be carefully investigated considering that PAD4 may have other functions on transcriptional regulation via epigenetic mechanisms[40]. Studies to date have employed DNase I, which can effectively degrade NETs *in vivo*, to directly implicate the role of NETs in various experimental disease models[7, 36]. It has been shown that targeting NETs with DNase I could accelerate wound healing[7] and treat disorders such as kidney injury[41], systemic lupus erythematosus (SLE)[42], inflammation-associated vascular occlusion[43] and cancer metastasis[44]. Moreover, DNase I (Pulmozyme®) has been utilized clinically as a *bona fide* first line of treatment for cystic fibrosis without notable side effects[45]. Disruption of NETs, however, could impede the capacity of neutrophils to prevent commensal dissemination or eliminate the invading pathogen during leaky guts or GI infection, respectively. Herein, we observed that DNase I treatment indeed aggravated the pathogen burden in the colon, ceca and spleen, and worsened colonic inflammation and hyperplasia. This suggests that the mucoprotective feature of PAD4 could be primarily mediated through formation of NETs, though further studies should consider whether other non-NETs-related role of PAD4 may also be involved in conferring protection against *CR*. However, administration of the PAD4 inhibitor, Cl-amidine, resulted in only a partial exacerbation of *CR* infection. Such outcomes suggest that *CR* infection could be aggravated by loss of NETs, but its severity may differ depending on the mode of NETs inhibition via genetic deficiency or pharmacological intervention. It is tempting to speculate that a higher dose of Cl-amidine may be required in order to recapitulate the severe disease observed in *CR*-infected *Pad4*$^{-/-}$ mice and DNase I-treated mice. Nevertheless, the exacerbation of disease in mice given DNase I or Cl-amidine argue that NETs dysregulation is detrimental in the context of GI infection.

Taken together, our findings were in contrast with other reports demonstrating the beneficial effects of PAD4 inhibition in alleviating the severity of inflammatory arthritis[46], promoting survival during sepsis[47, 48] and ameliorating SLE[49], atherosclerosis[50] and dextran sodium sulfate-induce colitis in mice[51]. Such disparity suggests that the effects of PAD4 may be context-dependent and varied according to underlying causative agent(s) of the disease. It is possible that NETs formed against *CR* infection may have adverse effects to some extent, but such effects are outweighed by its protective role in limiting pathogen burden and dissemination. Further studies are certainly warranted to determine whether inhibiting PAD4 could have detrimental effects against other systemic or localized infection(s) mediated by various pathogens. It would be important for future studies to also consider the contribution of other non-canonical NETs formation, e.g. PAD4-independent NETosis and mitochondrial NETosis[52], against bacterial infection. Collectively, our study underscores the critical role of PAD4 at the mucosal surfaces during enteropathogen infection.

METHODS

Reagents

Histopaque-1077 and −1119, RPMI 1640, Luria-Bertani (LB) broth, bovine serum albumin (BSA), paraformaldehyde, nalidixic acid and kanamycin were procured from Sigma (St. Louis, MO). DNase I (dornase alfa, Pulmozyme®) was kindly gifted from Genentech. Duoset enzyme-linked immunosorbent assay (ELISA) kits for mouse Lipocalin2 (Lcn2), keratinocyte-derived chemokine (KC), serum amyloid A (SAA), neutrophil elastase (NE), myeloperoxidase (MPO), interleukin (IL)-22 and IL-17A were obtained from R&D Systems (Minneapolis, MN). SYBR Green mix and the qScript complementary DNA (cDNA) synthesis kit were procured from Quanta BioSciences (Gaithersburg, MD). Ly6G antibody was purchased from Abcam (Cambridge, MA). All other fine chemicals used in the present study were reagent grade and procured from Sigma. Alcian Blue (pH 2.5) Stain Kit was obtained from Vector Laboratories (Burlingame, CA). Mouse Lamina Propria Dissociation Kit was purchased from Miltenyi Biotec (Auburn, CA). Cl-amidine (hydrochloride) was obtained from Cayman chemicals (Ann Arbor, MI).

Mice

Pad4$^{-/-}$ mice on C57BL/6 background was generated by Dr. Yanming Wang (Pennsylvania State University, University Park, PA) and bred with BL/6 wild type (WT) mice in our colony. The resulting offspring were crossed to generate homozygous *Pad4*$^{-/-}$ mice and their WT littermates. These mice were bred in-house in the animal facility at University of Toledo and Pennsylvania State University under SPF conditions. All of the mice are on the C57BL/6 (BL6) background and were crossed with BL6 WT mice for >10 generations. This study was performed in strict accordance with the recommendations in the Guide for the Care and Use of Laboratory Animals of the National Institutes of Health and was approved by the Institutional Animal Care and Use Committee (IACUC) at The Pennsylvania State University and University of Toledo.

C. rodentium infection

C. rodentium strain ICC169 (nalidixic acid-resistant) and bioluminescent strain ICC180 (kanamycin-resistant) were kind gifts from Dr. Gad Frankel (London School of Medicine and Dentistry, London, United Kingdom) via Dr. Margherita T. Cantorna (Pennsylvania State University, University Park, PA). The ICC169 strain was cultured in Luria-Bertani (LB, Sigma) broth containing 50 μg/ml nalidixic acid (Sigma), whereas the ICC180 strain was cultured in LB broth containing 100 μg/ml kanamycin (Sigma). *Pad4*$^{-/-}$ mice and their WT littermates (male, 8 weeks) were infected by oral gavage with $1X10^9$ colony forming unit (CFU) in 100 μl of PBS. Mice were monitored for body weight and euthanized at 10 and 28 days of p.i. To monitor *CR* fecal shedding and dissemination, feces and other tissues were collected, homogenized and plated in serial dilutions on LB agar plates containing nalidixic acid. Plates were incubated overnight at 37°C for CFU counting.

For *in vivo* infection kinetics study, $1X10^{10}$ CFU of *C. rodentium* ICC180 was used. WT and *Pad4*$^{-/-}$ mice were fed with alfalfa-free purified diet (Research Diets Inc., New Brunswick, NJ) to minimize the background luminescence from chlorophyll present in grain-based chow. Following infection, the animals were imaged every other day using the IVIS spectrum animal imaging system (Xenogen Corp., Alameda, CA, USA). Images were analyzed by Living Image software (PerkinElmer, Waltham, MA). Feces and other tissues were collected, homogenized and plated in serial dilutions on LB agar plates containing kanamycin and CFU were quantified.

DNase I treatment

Pad4$^{-/-}$ mice and their WT littermates (male, 8 weeks) were administered 50 μg i.p. DNase I (dornase alfa, Genentech) 3h after *CR* infection and once daily for the next 3 consecutive days and then once every alternate day until day 11. Control mice were given 100 μl of vehicle control (8.77 mg/ml NaCl and 0.15 mg/ml $CaCl_2$)[7].

Inhibiting PAD4 via Cl-amidine treatment

Pad4$^{-/-}$ mice and their WT littermates (male, 8 weeks) were administered Cl-amidine (20 mg/kg b.wt/mice) i.p. 3h prior to *CR* infection, followed by daily injections for the next 3 consecutive days and then once every alternate day until day 11. Control mice were given 100 μl of vehicle control (PBS, 1X).

Euthanasia and blood collection

At termination of the experiment, mice were euthanized via CO_2 asphyxiation and analyzed for standard colitis parameters. Blood was collected at the time of euthanasia in BD microtainers (Becton, Dickinson) via cardiac puncture. Hemolysis-free serum was obtained after centrifugation and stored at -80^oC until further analysis.

Quantifying *C. rodentium* CFU

Fecal samples from *CR*-infected mice were collected, weighed and then homogenized in sterile phosphate-buffered saline (PBS, 100 mg/ml). Cecal content, mesenteric lymph nodes (MLNs) and spleen were aseptically collected and homogenized in PBS (100 mg/ml). The

homogenates were centrifuged at 200 rpm for 1 min, serially diluted and plated (100 μl) on LB agar plates containing either nalidixic acid or kanamycin. Plates were incubated overnight at 37°C and the CFU was counted.

Quantitative Reverse-Transcriptase Polymerase Chain Reaction

Distal colons were collected in RNAlater (Sigma) and stored in −80°C. Total mRNA was extracted by using Trizol reagent (Sigma) as described in the manufacturer's protocol. mRNA (0.5 μg) was used to synthesize cDNA for qRT-PCR using SYBR green (Quanta) according to manufacturer's protocol. The sequences of primers used for quantitative reverse-transcriptase polymerase chain reaction were (sense and antisense, respectively): *KC* 5'-TTGTGCGAAAAGAAGTGCAG −3', and 5'-TACAAACACAGCCTCCCACA −3'; tumor necrosis factor alpha (*TNF-α*) 5'-ACTCCAGGCGGTGCCTATGT −3' and 5'-AGTGTGAGGGTCTGGGCCAT −3'; *iNOS* 5'-TTTGCTTCCATGCTAATGCGAAAG −3', and 5'-GCTCTGTTGAGGTCTAAAGGCTCCG −3'[53]; *IL-6* 5'-ACAACGATGATGCACTT-3' and 5'-CTTGGTCCTTAGCCACT-3'; *IL-17* 5'-TCATCCCTCAAAGCTCAGCG −3' and 5'-TTTCCCTCCGCATTGACAGA-3'; *IFN-γ* 5'-TCAAGTGGCATAGATGTGG-3' and 5'-TGGCTCTGCAGGATTTTCAT-3'; *IL-1β* 5'-TTGACGGACCCCAAAAGAT-3' and 5'-AGAAGGTGCTCATGTCCTG-3'and *36B4* 5'-TCCAGGCTTTGGGCATCA-3' and 5'-CTT TATTCAGCTGCACATCACTCAGA-3'[19]. *36B4* was used to normalize relative mRNA expression using Ct ($2^{\Delta\Delta Ct}$) method. Fold change was determined by comparison to the untreated control group.

Enzyme-linked immunosorbent assay (ELISA)

Reconstitution of fecal samples was performed as described previously[19]. Briefly, frozen or freshly collected feces were reconstituted in PBS containing 0.1% Tween 20 to make 100 mg/ml fecal suspension and vortexed for 30 min at room temperature. Fecal suspensions were centrifuged at 4°C for 10,000g for 10 min and the clear supernatants were collected. Samples from *CR*-infected mice were titrated for optimal dilution, whereas samples from controls were diluted 1:10 to be analyzed for fecal lipocalin 2 (Lcn2) using Duoset ELISA kits according to manufacturer instructions. Fecal IgA was measured via ELISA using standard procedures as described previously[54]. Polygonal goat anti-mouse IgA and HRP-conjugated goat anti-mouse IgA (Southern Biotechnology) were used as capture and detection antibody, respectively. A standard curve was generated using mouse IgA (κ isotype) control mAb (BD Biosciences).

Hemolysis-free sera were collected from *CR*-infected WT and *Pad4*$^{-/-}$ mice. Lcn2, serum amyloid A (SAA), keratinocyte-derived chemoattractant (KC, alias CXCL1), neutrophil elastase (NE) and myeloperoxidase (MPO) were measured in serum via Duoset ELISA kits from R&D Systems. Colonic samples were homogenized in RIPA buffer (100 mg/ml, Cell Signaling) containing 1x protease inhibitor cocktail (Roche) and were centrifuged at 4^{O}C at 12,000g for 10 min. The clear supernatants were collected, diluted and analysed using IL-22 and IL-17A Duoset ELISA kits according to the manufacturer instructions.

Serum immunoreactivity to bacterial proteins

E. coli (K12 strain) was grown overnight in Luria Bertani (LB) medium, pelleted by centrifugation and lysed in RIPA buffer (Cell Signaling) with protease inhibitor cocktail (1X, Roche). Lysates (40 μg protein per lane) were fractionated via SDS-PAGE. Proteins were transferred to PVDF membrane and probed with sera (1:1000) from control either *CR*-infected WT or *Pad4*$^{-/-}$ mice for overnight at 4°C, followed by 1h incubation with anti-mouse HRP (1:000). Immunoblot was developed by LI-COR Odyssey CLX method.

Lamina propria immune cells isolation

Colonic tissues from controls and *CR*-infected WT and *Pad4*$^{-/-}$ mice were dissociated to single-cell suspensions by combining mechanical dissociation and enzymatic degradation, followed by lamina propria immune cells isolation according to manufacturer's instructions (mouse Lamina Propria Dissociation Kit, Miltenyi Biotec).

Flow cytometric characterization of lamina propria immune cells

Lamina propria immune cells (2.0×10^5/200 μl) were stained with fluorophore-conjugated anti-mouse monoclonal antibodies (BD Bioscience), directed against the following cell surface proteins: CD3-PE and CD4-PE-Cy7, in staining buffer (BD Bioscience) and incubated for 30 min at room temperature in the dark. After surface staining, cells were washed in PBS, fixed and permeabilized with FoxP3 Staining Buffer Kit (BD Bioscience) according to manufacturer's instructions and incubated with FoxP3-Alexa Fluor 488 and RORγt-Alexa Fluor 647 for 1h at room temperature. Cells were washed twice in FACS Buffer and were analyzed by Accuri c6 flow cytometer (BD Biosciences) with BD Accuri C6 Software (Becton Dickinson). Immune cells were defined by using surface markers: regulatory T cells (Treg) $CD3^+CD4^+FoxP3^+$; Th17 cells $CD3^+CD4^+ROR\gamma t^+$.

Histology and Immunohistochemistry

Colons from control and *CR*-infected mice were washed with PBS to get rid of fecal contents and opened longitudinally along the mesenteric border and Swiss-rolled from the proximal to distal end. The Swiss-rolls were placed in 10% neutral-buffered formalin for 24 h and transferred to 70% ethanol, and processed to generate 5 μm sections for histochemical and immunohistochemical staining. Hematoxylin & eosin staining were performed to observe the morphological and histopathological changes like crypt structure, ulceration and crypt loss, epithelial hyperplasia, mucosal thickening, and extent of immune cell infiltration (ICI) in mucosa and submucosa. To stain acidic mucin in the goblet cells, Alcian blue staining (pH 2.5) was performed using a Kit from Vector Laboratories (Burlingame, CA).

To detect NETs, colon sections were deparaffinized, antigen-retrieved, permeabilized and then blocked with 10% donkey serum. Subsequently, the sections were incubated with rat anti-neutrophil Ly6G (1:500, Abcam) and rabbit anti-citrullinated histone 3 (citrulline R2 + R8 + R17) antibody (1:200, Abcam) overnight at 4°C. After washing with PBS, the sections were incubated with donkey anti-rat Alexa Fluor 594 and donkey anti-rabbit Alexa Fluor 488 conjugated antibody (Invitrogen/ThermoFisher Scientific) for 1h at RT. Sections were mounted with Fluoroshield™ DAPI (Sigma) and imaged via using VS120 Virtual Slide Microscope (Olympus) and the OlyVIA software.

The apoptotic cells were detected via TUNEL labeling as per manufacturers protocol (*In Situ* Cell Death Detection Kit, Roche/Millipore Sigma). The TUNEL-stained sections were mounted with Fluoroshield™ DAPI (Sigma) and imaged via using VS120 Virtual Slide Microscope (Olympus) and the OlyVIA software.

Statistics

All data were represented as mean ± SEM. The statistical significance between two groups was calculated using unpaired, two-tailed t-test. Data from more than two groups was compared using a one-way ANOVA followed by Tukey's multiple comparison tests (when to compare the mean of each column with the mean of every other column). The p values <0.05 were considered statistically significant and are denoted as *$p < 0.05$, **$p < 0.01$, and ***$p < 0.001$. All statistical analyses were performed with GraphPad Prism 7.0 software (GraphPad, La Jolla, CA).

Supplementary Material

Refer to Web version on PubMed Central for supplementary material.

Acknowledgements:

This work was supported by a grant from the National Institutes of Health (www.nih.gov; grant R01 DK097865) to MVK. P.S. (Ref.# 522820) and V.S (Ref# 418507) are supported by Crohn's & Colitis Foundation of America (CCFA) Research Fellowship Award (www.crohnscolitisfoundation.org). We thank Genentech Inc. (San Francisco, CA) for kindly providing DNase I.

References

1. Brinkmann V, Reichard U, Goosmann C, Fauler B, Uhlemann Y, Weiss DS et al. Neutrophil extracellular traps kill bacteria. Science 2004; 303(5663): 1532–1535 [PubMed: 15001782]
2. Fuchs TA, Abed U, Goosmann C, Hurwitz R, Schulze I, Wahn V et al. Novel cell death program leads to neutrophil extracellular traps. The Journal of cell biology 2007; 176(2): 231–241. [PubMed: 17210947]
3. Parker H, Dragunow M, Hampton MB, Kettle AJ, Winterbourn CC. Requirements for NADPH oxidase and myeloperoxidase in neutrophil extracellular trap formation differ depending on the stimulus. Journal of leukocyte biology 2012; 92(4): 841–849. [PubMed: 22802447]
4. Arazna M, Pruchniak MP, Demkow U. Reactive Oxygen Species, Granulocytes, and NETosis. Advances in experimental medicine and biology 2015; 836: 1–7. [PubMed: 25310939]
5. Wang Y, Li M, Stadler S, Correll S, Li P, Wang D et al. Histone hypercitrullination mediates chromatin decondensation and neutrophil extracellular trap formation. The Journal of cell biology 2009; 184(2): 205–213. [PubMed: 19153223]
6. Li P, Li M, Lindberg MR, Kennett MJ, Xiong N, Wang Y. PAD4 is essential for antibacterial innate immunity mediated by neutrophil extracellular traps. The Journal of experimental medicine 2010; 207(9): 1853–1862. [PubMed: 20733033]
7. Wong SL, Demers M, Martinod K, Gallant M, Wang Y, Goldfine AB et al. Diabetes primes neutrophils to undergo NETosis, which impairs wound healing. Nat Med 2015; 21(7): 815–819. [PubMed: 26076037]
8. Martinod K, Demers M, Fuchs TA, Wong SL, Brill A, Gallant M et al. Neutrophil histone modification by peptidylarginine deiminase 4 is critical for deep vein thrombosis in mice. Proceedings of the National Academy of Sciences of the United States of America 2013; 110(21): 8674–8679 [PubMed: 23650392]

9. Martinod K, Fuchs TA, Zitomersky NL, Wong SL, Demers M, Gallant M et al. PAD4-deficiency does not affect bacteremia in polymicrobial sepsis and ameliorates endotoxemic shock. Blood 2015; 125(12): 1948–1956. [PubMed: 25624317]
10. Savchenko AS, Borissoff JI, Martinod K, De Meyer SF, Gallant M, Erpenbeck L et al. VWF-mediated leukocyte recruitment with chromatin decondensation by PAD4 increases myocardial ischemia/reperfusion injury in mice. Blood 2014; 123(1): 141–148. [PubMed: 24200682]
11. Huang H, Tohme S, Al-Khafaji AB, Tai S, Loughran P, Chen L et al. Damage-associated molecular pattern-activated neutrophil extracellular trap exacerbates sterile inflammatory liver injury. Hepatology 2015; 62(2): 600–614. [PubMed: 25855125]
12. Wales AD, Woodward MJ, Pearson GR. Attaching-effacing bacteria in animals. J Comp Pathol 2005; 132(1): 1–26. [PubMed: 15629476]
13. Bouladoux N, Harrison OJ, Belkaid Y. The Mouse Model of Infection with Citrobacter rodentium. Current protocols in immunology / edited by John E Coligan [et al] 2017; 119: 19 15 11–19 15 25.
14. Barthold SW, Coleman GL, Jacoby RO, Livestone EM, Jonas AM. Transmissible murine colonic hyperplasia. Vet Pathol 1978; 15(2): 223–236. [PubMed: 664189]
15. Schauer DB, Falkow S. Attaching and effacing locus of a Citrobacter freundii biotype that causes transmissible murine colonic hyperplasia. Infection and immunity 1993; 61(6): 2486–2492. [PubMed: 8500884]
16. Collins JW, Keeney KM, Crepin VF, Rathinam VA, Fitzgerald KA, Finlay BB et al. Citrobacter rodentium: infection, inflammation and the microbiota. Nature reviews Microbiology 2014; 12(9): 612–623. [PubMed: 25088150]
17. Lebeis SL, Bommarius B, Parkos CA, Sherman MA, Kalman D. TLR signaling mediated by MyD88 is required for a protective innate immune response by neutrophils to Citrobacter rodentium. Journal of immunology 2007; 179(1): 566–577.
18. Lee YS, Yang H, Yang JY, Kim Y, Lee SH, Kim JH et al. Interleukin-1 (IL-1) signaling in intestinal stromal cells controls KC/CXCL1 secretion, which correlates with recruitment of IL-22-secreting neutrophils at early stages of Citrobacter rodentium infection. Infection and immunity 2015; 83(8): 3257–3267. [PubMed: 26034212]
19. Chassaing B, Srinivasan G, Delgado MA, Young AN, Gewirtz AT, Vijay-Kumar M. Fecal lipocalin 2, a sensitive and broadly dynamic non-invasive biomarker for intestinal inflammation. PloS one 2012; 7(9): e44328. [PubMed: 22957064]
20. Aujla SJ, Chan YR, Zheng M, Fei M, Askew DJ, Pociask DA et al. IL-22 mediates mucosal host defense against Gram-negative bacterial pneumonia. Nat Med 2008; 14(3): 275–281. [PubMed: 18264110]
21. Zheng Y, Valdez PA, Danilenko DM, Hu Y, Sa SM, Gong Q et al. Interleukin-22 mediates early host defense against attaching and effacing bacterial pathogens. Nat Med 2008; 14(3): 282–289. [PubMed: 18264109]
22. Frankel G, Phillips AD, Novakova M, Field H, Candy DC, Schauer DB et al. Intimin from enteropathogenic Escherichia coli restores murine virulence to a Citrobacter rodentium eaeA mutant: induction of an immunoglobulin A response to intimin and EspB. Infection and immunity 1996; 64(12): 5315–5325. [PubMed: 8945583]
23. Maaser C, Housley MP, Iimura M, Smith JR, Vallance BA, Finlay BB et al. Clearance of Citrobacter rodentium requires B cells but not secretory immunoglobulin A (IgA) or IgM antibodies. Infection and immunity 2004; 72(6): 3315–3324. [PubMed: 15155635]
24. Luperchio SA, Schauer DB. Molecular pathogenesis of Citrobacter rodentium and transmissible murine colonic hyperplasia. Microbes and infection 2001; 3(4): 333–340. [PubMed: 11334751]
25. Bergstrom KS, Guttman JA, Rumi M, Ma C, Bouzari S, Khan MA et al. Modulation of intestinal goblet cell function during infection by an attaching and effacing bacterial pathogen. Infection and immunity 2008; 76(2): 796–811. [PubMed: 17984203]
26. Leshner M, Wang S, Lewis C, Zheng H, Chen XA, Santy L et al. PAD4 mediated histone hypercitrullination induces heterochromatin decondensation and chromatin unfolding to form neutrophil extracellular trap-like structures. Frontiers in immunology 2012; 3: 307. [PubMed: 23060885]

27. Luo Y, Arita K, Bhatia M, Knuckley B, Lee YH, Stallcup MR et al. Inhibitors and inactivators of protein arginine deiminase 4: functional and structural characterization. Biochemistry 2006; 45(39): 11727–11736. [PubMed: 17002273]
28. Koroleva EP, Halperin S, Gubernatorova EO, Macho-Fernandez E, Spencer CM, Tumanov AV. Citrobacter rodentium-induced colitis: A robust model to study mucosal immune responses in the gut. J Immunol Methods 2015; 421: 61–72. [PubMed: 25702536]
29. Conlan JW. Critical roles of neutrophils in host defense against experimental systemic infections of mice by Listeria monocytogenes, Salmonella typhimurium, and Yersinia enterocolitica. Infection and immunity 1997; 65(2): 630–635. [PubMed: 9009323]
30. Crepin VF, Habibzay M, Glegola-Madejska I, Guenot M, Collins JW, Frankel G. Tir Triggers Expression of CXCL1 in Enterocytes and Neutrophil Recruitment during Citrobacter rodentium Infection. Infection and immunity 2015; 83(9): 3342–3354. [PubMed: 26077760]
31. Gibson DL, Ma C, Rosenberger CM, Bergstrom KS, Valdez Y, Huang JT et al. Toll-like receptor 2 plays a critical role in maintaining mucosal integrity during Citrobacter rodentium-induced colitis. Cellular microbiology 2008; 10(2): 388–403. [PubMed: 17910742]
32. Khan MA, Ma C, Knodler LA, Valdez Y, Rosenberger CM, Deng W et al. Toll-like receptor 4 contributes to colitis development but not to host defense during Citrobacter rodentium infection in mice. Infection and immunity 2006; 74(5): 2522–2536. [PubMed: 16622187]
33. Buschor S, Cuenca M, Uster SS, Scharen OP, Balmer ML, Terrazos MA et al. Innate immunity restricts Citrobacter rodentium A/E pathogenesis initiation to an early window of opportunity. PLoS pathogens 2017; 13(6): e1006476. [PubMed: 28662171]
34. Spehlmann ME, Dann SM, Hruz P, Hanson E, McCole DF, Eckmann L. CXCR2-dependent mucosal neutrophil influx protects against colitis-associated diarrhea caused by an attaching/effacing lesion-forming bacterial pathogen. Journal of immunology 2009; 183(5): 3332–3343.
35. Halverson TW, Wilton M, Poon KK, Petri B, Lewenza S. DNA is an antimicrobial component of neutrophil extracellular traps. PLoS pathogens 2015; 11(1): e1004593. [PubMed: 25590621]
36. Kolaczkowska E, Jenne CN, Surewaard BG, Thanabalasuriar A, Lee WY, Sanz MJ et al. Molecular mechanisms of NET formation and degradation revealed by intravital imaging in the liver vasculature. Nature communications 2015; 6: 6673.
37. O'Brien XM, Biron BM, Reichner JS. Consequences of extracellular trap formation in sepsis. Curr Opin Hematol 2017; 24(1): 66–71. [PubMed: 27820735]
38. Backert I, Koralov SB, Wirtz S, Kitowski V, Billmeier U, Martini E et al. STAT3 activation in Th17 and Th22 cells controls IL-22-mediated epithelial host defense during infectious colitis. Journal of immunology 2014; 193(7): 3779–3791.
39. Vallance BA, Deng W, Knodler LA, Finlay BB. Mice lacking T and B lymphocytes develop transient colitis and crypt hyperplasia yet suffer impaired bacterial clearance during Citrobacter rodentium infection. Infection and immunity 2002; 70(4): 2070–2081. [PubMed: 11895973]
40. Wang Y, Wysocka J, Sayegh J, Lee YH, Perlin JR, Leonelli L et al. Human PAD4 regulates histone arginine methylation levels via demethylimination. Science 2004; 306(5694): 279–283. [PubMed: 15345777]
41. Cedervall J, Dragomir A, Saupe F, Zhang Y, Arnlov J, Larsson E et al. Pharmacological targeting of peptidylarginine deiminase 4 prevents cancer-associated kidney injury in mice. Oncoimmunology 2017; 6(8): e1320009. [PubMed: 28919990]
42. Davis JC Jr., Manzi S, Yarboro C, Rairie J, McInnes I, Averthelyi D et al. Recombinant human Dnase I (rhDNase) in patients with lupus nephritis. Lupus 1999; 8(1): 68–76. [PubMed: 10025601]
43. Jimenez-Alcazar M, Rangaswamy C, Panda R, Bitterling J, Simsek YJ, Long AT et al. Host DNases prevent vascular occlusion by neutrophil extracellular traps. Science 2017; 358(6367): 1202–1206. [PubMed: 29191910]
44. Park J, Wysocki RW, Amoozgar Z, Maiorino L, Fein MR, Jorns J et al. Cancer cells induce metastasis-supporting neutrophil extracellular DNA traps. Science translational medicine 2016; 8(361): 361ra138.
45. Thomson AH. Human recombinant DNase in cystic fibrosis. J R Soc Med 1995; 88 Suppl 25: 24–29.

46. Willis VC, Gizinski AM, Banda NK, Causey CP, Knuckley B, Cordova KN et al. N-alpha-benzoyl-N5-(2-chloro-1-iminoethyl)-L-ornithine amide, a protein arginine deiminase inhibitor, reduces the severity of murine collagen-induced arthritis. Journal of immunology 2011; 186(7): 4396–4404.

47. Li Y, Liu Z, Liu B, Zhao T, Chong W, Wang Y et al. Citrullinated histone H3: a novel target for the treatment of sepsis. Surgery 2014; 156(2): 229–234. [PubMed: 24957671]

48. Biron BM, Chung CS, O'Brien XM, Chen Y, Reichner JS, Ayala A. Cl-Amidine Prevents Histone 3 Citrullination and Neutrophil Extracellular Trap Formation, and Improves Survival in a Murine Sepsis Model. J Innate Immun 2017; 9(1): 22–32. [PubMed: 27622642]

49. Knight JS, Zhao W, Luo W, Subramanian V, O'Dell AA, Yalavarthi S et al. Peptidylarginine deiminase inhibition is immunomodulatory and vasculoprotective in murine lupus. The Journal of clinical investigation 2013; 123(7): 2981–2993. [PubMed: 23722903]

50. Knight JS, Luo W, O'Dell AA, Yalavarthi S, Zhao W, Subramanian V et al. Peptidylarginine deiminase inhibition reduces vascular damage and modulates innate immune responses in murine models of atherosclerosis. Circ Res 2014; 114(6): 947–956. [PubMed: 24425713]

51. Chumanevich AA, Causey CP, Knuckley BA, Jones JE, Poudyal D, Chumanevich AP et al. Suppression of colitis in mice by Cl-amidine: a novel peptidylarginine deiminase inhibitor. Am J Physiol Gastrointest Liver Physiol 2011; 300(6): G929–938. [PubMed: 21415415]

52. Sorensen OE, Borregaard N. Neutrophil extracellular traps - the dark side of neutrophils. The Journal of clinical investigation 2016; 126(5): 1612–1620. [PubMed: 27135878]

53. Saha P, Chassaing B, Yeoh BS, Viennois E, Xiao X, Kennett MJ et al. Ectopic Expression of Innate Immune Protein, Lipocalin-2, in Lactococcus lactis Protects Against Gut and Environmental Stressors. Inflammatory bowel diseases 2017; 23(7): 1120–1132. [PubMed: 28445245]

54. Knoop KA, Kumar N, Butler BR, Sakthivel SK, Taylor RT, Nochi T et al. RANKL is necessary and sufficient to initiate development of antigen-sampling M cells in the intestinal epithelium. Journal of immunology 2009; 183(9): 5738–5747.

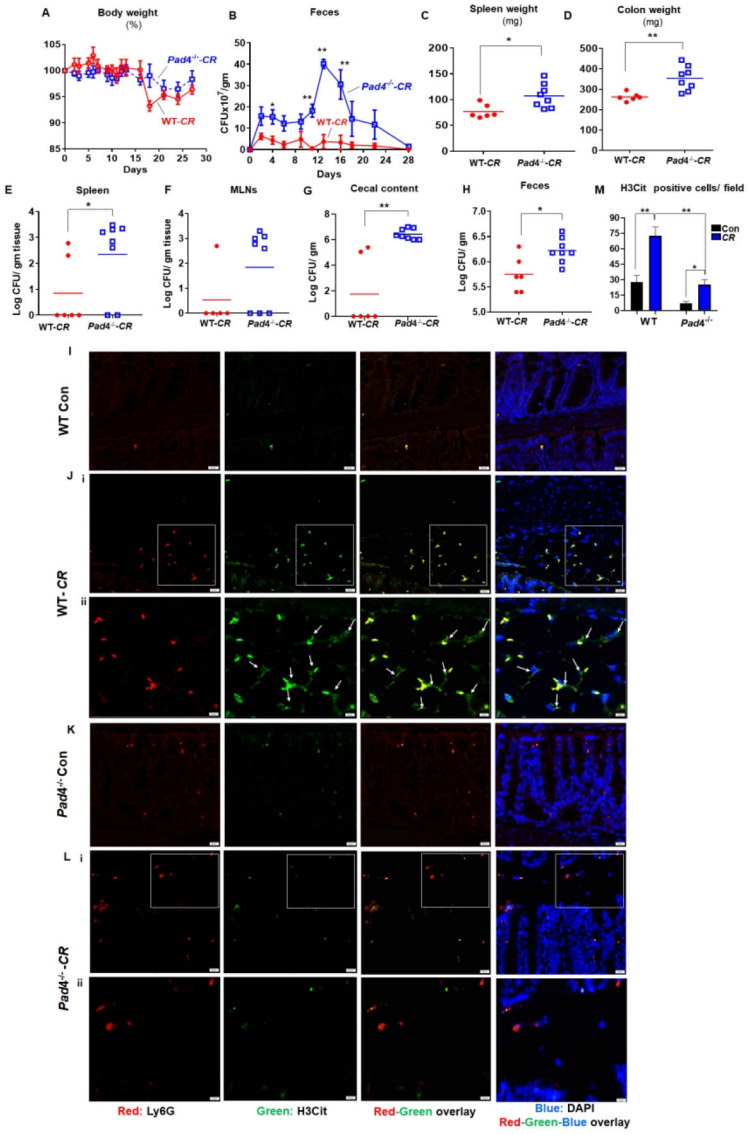

Fig. 1. Loss of PAD4 aggravated *C. rodentium* infection in mice.

Pad4$^{-/-}$ mice and their WT littermates (male, 8 weeks, n=6–8) were infected with 1X10^9 colony formation unit (CFU) of *C. rodentium* (*CR*) by oral gavage. Mice were monitored for (**A**) body weight and euthanized at day 28 post-infection (p.i.). (**B**) Fecal shedding of *CR* was determined at different time points. The following parameters were analyzed: (**C**) spleen weight and (**D**) colon weight. Bacterial dissemination was determined in (**E**) spleen, (**F**) mesenteric lymph nodes (MLNs), (**G**) cecal content and (**H**) fecal samples at day 28 p.i.. Colon swiss-roll sections from control and *CR*-infected (day 28 p.i) *Pad4*$^{-/-}$ mice and their WT littermates (male, 8 weeks, n=6–8) (proximal to distal portion) were used for NETs staining. Representative images of NETs visualized by costaining of Ly6G (red), H3Cit (green) and DNA (DAPI, blue) in (**I**) WT control, (**J**) *CR*-infected WT mice, (**K**) *Pad4*$^{-/-}$ control and (**L**) *CR*-infected *Pad4*$^{-/-}$ mice. The boxed regions in [J (i), K (i)] are magnified and presented [J (ii), K (ii)] in (400x, scale bar =10 μm). Magnification for others are 200x, scale bar = 20 μm. (**M**) Bar graph represents the number of CitH3 positive cells scored in at

least 4 different microscopic fields (at 100x) for each mouse. Results are expressed as means ± SEM. * $p < 0.05$ and ** $p < 0.01$.

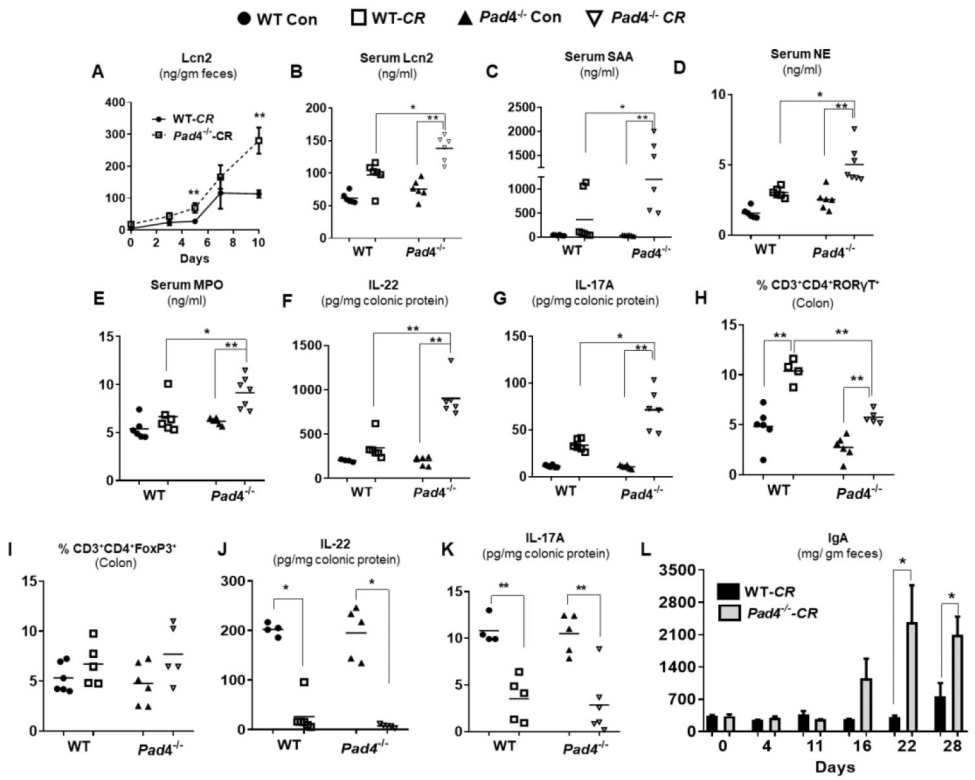

Fig. 2. PAD4 deficiency worsened the systemic and colonic inflammation in *C. rodentium* infected mice.

Fecal samples from *C. rodentium* (*CR*)-infected WT and *Pad4*$^{-/-}$ mice were analyzed for (**A**) Lipocalin 2 (Lcn2) at different time points up to day 10 p.i.. (**B**) serum Lcn2, (**C**) serum amyloid A (SAA), (**D**) neutrophil elastase (NE) and (**E**) myeloperoxidase (MPO) were analyzed in serum samples from *CR* infected WT and *Pad4*$^{-/-}$ mice. (**F**) IL-22 and (**G**) IL-17A levels were measured in colonic homogenates at day 10 p.i.. Control and *CR*-infected WT and *Pad4*$^{-/-}$ lamina propria immune cells were analysed for (**H**) % $CD3^+CD4^+ROR\gamma T^+$ Th17 cells, (**I**) % $CD3^+CD4^+FoxP3^+$ Treg cells by flow cytometry. Colonic (**J**) IL-22 and (**K**) IL-17A levels at day 28 p.i.. (**L**) Fecal IgA levels were determined by ELISA at different time points. Results are expressed as means ± SEM. *p< 0.05 and ** p<0.01.

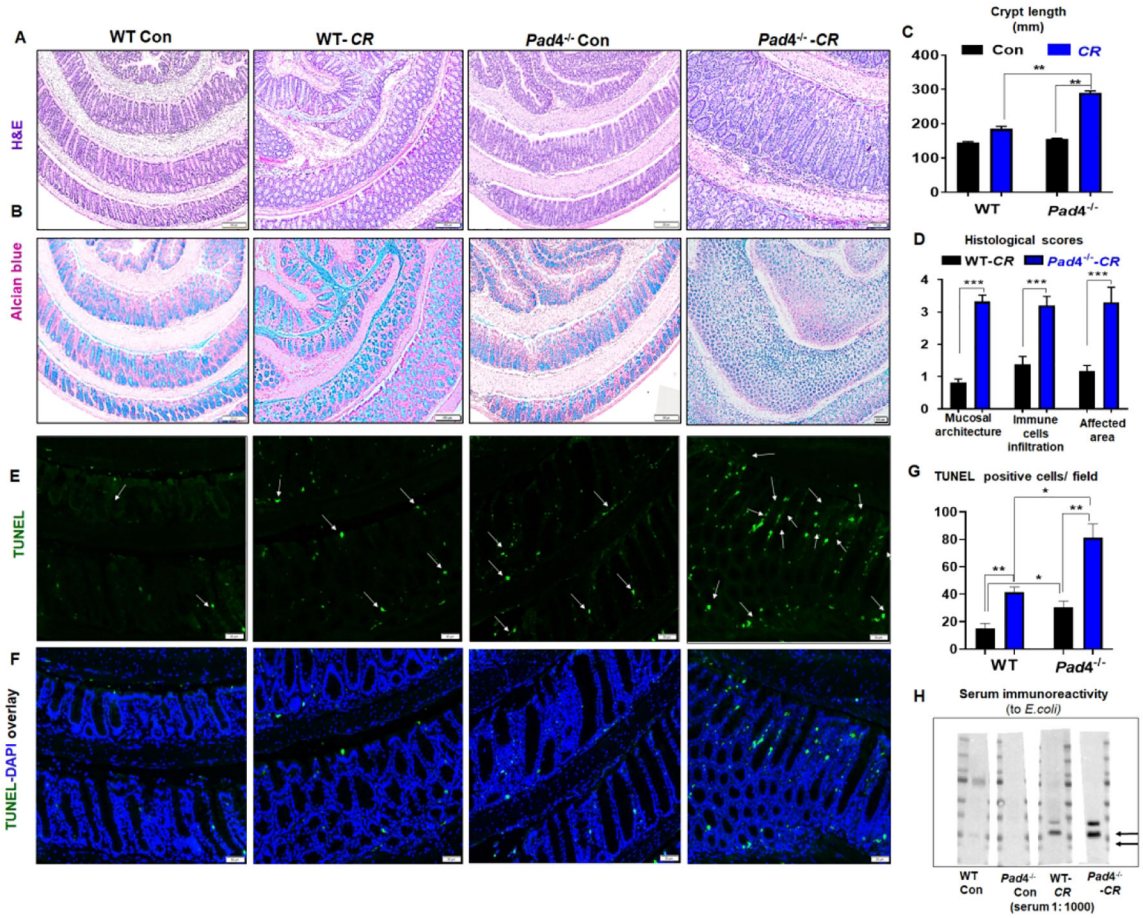

Fig. 3. *Pad4*-deficient mice displayed an aggravated colonic pathology following *C. rodentium* infection.

Colon from control and *C. rodentium* (*CR*)-infected (day 28 p.i.) *Pad4*$^{-/-}$ mice and their WT littermates (male, 8 weeks, n=6–8) (proximal to distal portion) were used for histochemical and immunohistochemical staining. (**A**) Hematoxylin and eosin (H&E) staining, (**B**) Alcian blue staining for goblet cells. (**C**) Bar graphs showing the crypt length. (**D**) Colonic histology was scored by visualizing the entire H&E-stained colon sections microscopically for the extent of epithelial hyperplasia, immune cells infiltration (ICI) in mucosa and submucosa, goblet cell loss, distortion of crypt structure, ulceration and crypt loss. Colon from control and *CR*-infected (day 28 p.i) WT and *Pad4*$^{-/-}$ mice were used for TUNEL staining. Representative images of (**E**) TUNEL-positive cells (green) in colonic crypts, (**F**) co-staining for TUNEL (green) and DNA (DAPI, blue). Arrows indicate TUNEL-positive cells. Magnification 200x, scale bar = 20 μm. (**G**) Bar graph represents the number of TUNEL positive cells scored in at least 4 different microscopic fields (at 100X) for each mouse. (**H**) Representative immunoblot showing serum immunoreactivity to *E. coli* proteins (arrows showing new bands/increased intensity in *CR*-infected *Pad4*$^{-/-}$ mice). Results are expressed as means ± SEM. * $p< 0.05$, ** $p<0.01$ and *** $p<0.001$.

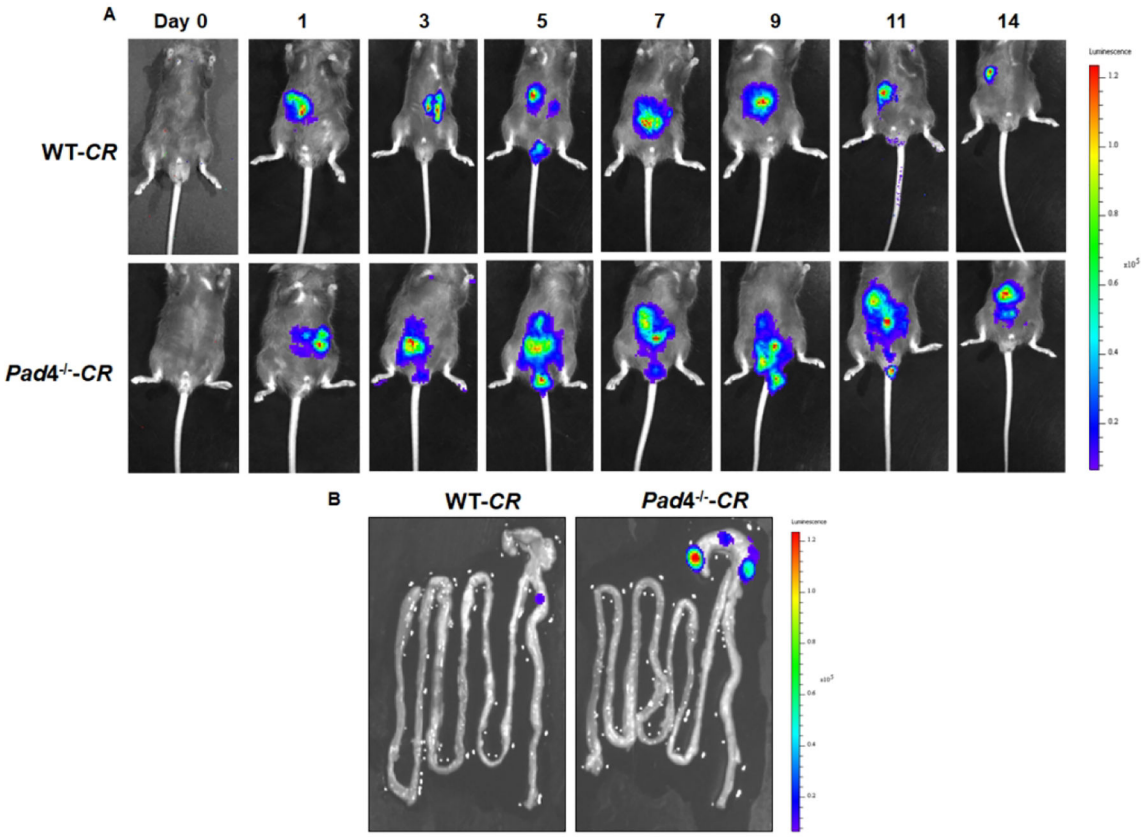

Fig. 4. *Pad4*$^{-/-}$ mice were more susceptible to *C. rodentium* infection than WT mice.

WT and *Pad4*$^{-/-}$ mice (male, 8 weeks, n=3) were intragastrically challenged with bioluminescent *C. rodentium* (1X10^{10} CFU). (**A**) Whole-body imaging of WT and *Pad4*$^{-/-}$ mice infected with bioluminescent *C. rodentium* (*CR*) that were taken every other day using the IVIS spectrum animal imaging system. The image shows one mouse from a total of three mice per treatment group. (**B**) Mice were euthanized at day 14 post-infection and analyzed for whole intestine using IVIS spectrum animal imaging system.

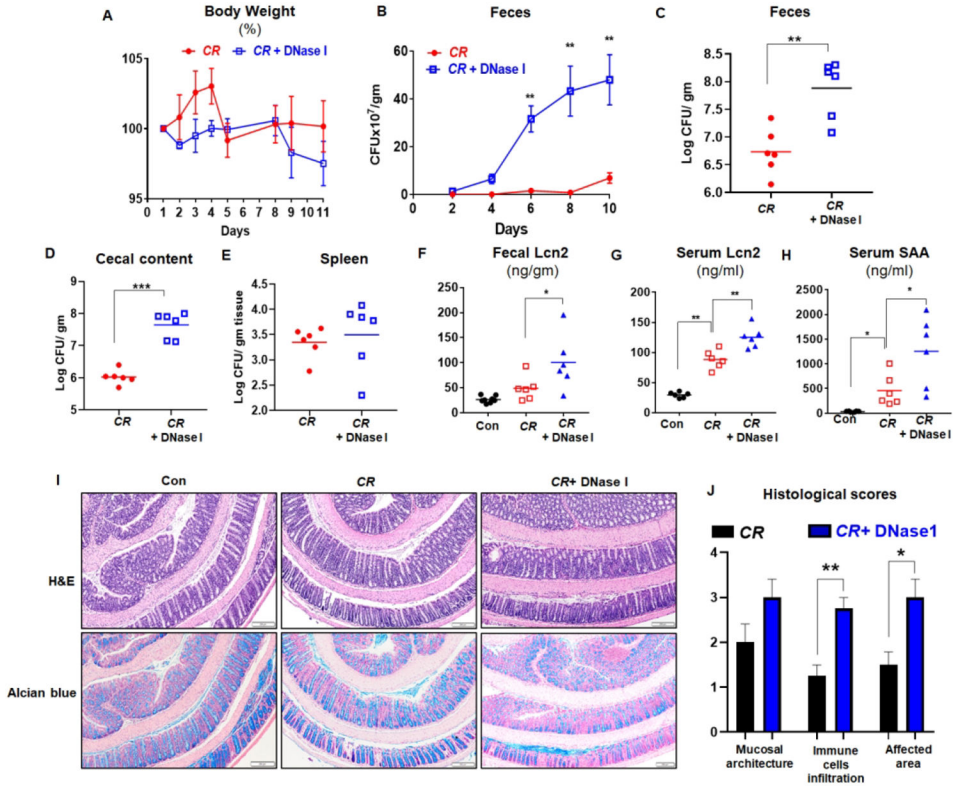

Fig. 5. DNase I treatment enhanced *C. rodentium* infection in WT mice.

WT mice (male, 8 weeks, n= 6) were infected with $1X10^9$ CFU of *C. rodentium* (*CR*) by oral gavage. One group of mice were treated with DNase I (dornase alfa, 50 μg/mice, i.p.) at 3h of post infection (p.i.), followed by once daily for the next 3 consecutive days and then once every alternative days. Mice were monitored for (**A**) body weight and (**B**) fecal shedding of *CR* (CFU) at different time points. Mice were euthanized at day 11 p.i. and *CR* burden was measured in (**C**) fecal samples, (**D**) cecal content and (**E**) spleen. (**F**) Fecal Lcn2, (**G**) serum Lcn2 and (**H**) SAA were determined by ELISA. (**I**) Colons (proximal to distal portion) were used for H&E staining, and Alcian blue staining for goblet cells. (**J**) Colonic histology was scored by visualizing the entire H&E-stained colon sections microscopically for the extent of epithelial hyperplasia, immune cells infiltration (ICI) in mucosa and submucosa, goblet cell loss, distortion of crypt structure, ulceration and crypt loss. Results are expressed as means ± SEM. * $p< 0.05$, ** $p<0.01$.

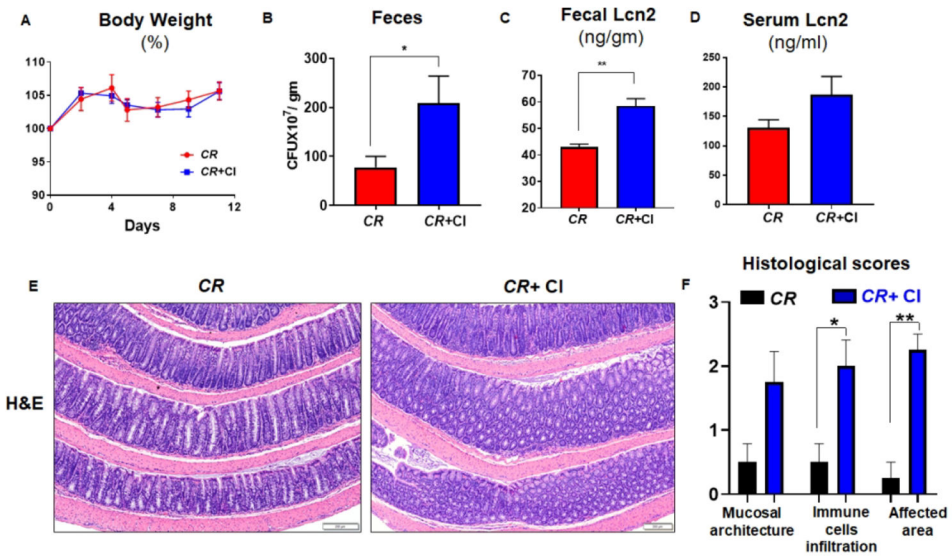

Fig. 6. Cl-amidine treatment modestly enhanced the susceptibility of *C. rodentium* infection in WT mice.

WT mice (male, 8 weeks, n= 6) were infected with $1X10^9$ CFU of *C. rodentium* (*CR*) by oral gavage. One group of mice were treated with Cl-amidine (20 mg/kg b.wt/mice, i.p.) at 3h prior to infection, followed by once daily for the next 3 consecutive days and then once every alternate days. Mice were monitored for (**A**) body weight and (**B**) fecal shedding of *CR* determined by CFU at day 11 p.i.. (**C**) Fecal Lcn2 and (**D**) serum Lcn2 were determined by ELISA. (**E**) Colons (proximal to distal portion) were used for H&E staining. (**F**) Colonic histology was scored by degree of epithelial hyperplasia, immune cells infiltration (ICI) in mucosa and submucosa, goblet cell loss, distortion of crypt structure, ulceration and crypt loss. Results are expressed as means ± SEM. * $p< 0.05$, ** $p<0.01$.